Journal of Engineering and Technology for Industrial Applications

ITEGAM-JETIA

Manaus, v.11 n.56, p.360-365. November/December, 2025.

DOI: https://doi.org/10.5935/jetia. v11i56.2890

ISSN ONLINE: 2447-0228

RESEARCH ARTICLE OPEN ACCESS

INFLUENCE OF IMPACT ANGLE ON MASS LOSS BEHAVIOUR OF SUPER 304HCu STAINLESS STEEL UNDER AIR JET EROSION CONDITIONS

M. Balachandar*[1] and M. Vinoth Kumar[2]

[1,2] Department of Mechanical Engineering, Hindustan Institute of Technology and Science, Chennai, Tamil Nadu, India - 603103.

[1]http://orcid.org/ 0000-0002-8223-4948, [2]http://orcid.org/0000-0003-2813-7095

Email: *balachandar2k1@gmail.com, vinothmecho@gmail.com

ARTICLE INFO

Article History
Received: November 5, 2025
Revised: November 20, 2025
Accepted: December 1, 2025
Published: December 31, 2025

Keywords:
Super 304HCu,
Boilers,
Air Jet Erosion,
Stainless steels.

ABSTRACT

Super 304HCu is a boiler-grade advanced austenitic stainless-steel material, used in heat exchangers for its resistance to oxidation and corrosion at high temperatures. The air jet erosion test is used to investigate the erosion behaviour of super 304HCu under various angles of impact. The samples are eroded in a test rig at different impact angles, under a constant impact velocity of 60 m/s and a particle feed rate of 3 g/min at ambient temperature, for 5 minutes. The mass loss is found to be 10 times higher at a low angle of impact (15°) than at the higher angles (>30°). The mass loss behaviour of the Super 304HCu is typical of a ductile material and the mass loss observed is compared with similar grades of stainless steel.

I. INTRODUCTION

Super 304HCu is a relatively new grade of austenitic stainless steel containing copper as an alloying element developed to provide adequate resistance to high-temperature oxidation and creep [1], [2]. Super 304HCu is used as a construction material in superheaters for ultra-supercritical boilers in the form of tubes and walls. Air jet erosion is a significant concern in power plant engineering systems, as it leads to material loss and surface degradation [3-5]. In coal-fired power plants, the boiler tubes and walls are prone to severe degradation by air jet erosion while coming in contact with high-velocity particulate matter like fly ash [6-8]. The mechanical interactions of particles with materials will cause severe material loss, and this can also be further complicated by erosion-corrosion interactions. Erosion in stainless steels is primarily caused by the mechanical action of solid particles impacting the material surface at high velocity. The variables like angle of impact, speed, particle size, and ductility of the material all affect the erosion rate of the material. An air jet erosion test can simulate erosive conditions in a laboratory environment, which involves using an air jet to propel abrasive particles at the material surface and measure the material loss [5].

It is effective in providing insights into the erosion mechanisms and the relative erosion resistance of different materials. The results from the air jet erosion test can help in understanding the material's behaviour under various impact angles, making it a valuable tool for assessing erosion performance [9], [10]. Erosion testing using air jets is a reliable method for evaluating the erosion resistance of materials, providing valuable data for understanding and improving material performance in erosive environments [11], [12]. The failure mechanisms during erosion wear are identified as lip formation, cutting, ploughing, spalling, and phase transformations, which are operative in different regions of wear [9], [13]. Many researchers had explored the relationship between mechanical properties such as hardness and erosion resistance and reported that increased hardness improved erosion resistance [13-15]. However, the number of studies on the erosion behaviour of Super304HCu is scanty. This paper investigates the effect of angle of impact on the erosive behaviour of Super 304HCu stainless steel in an air jet erosion test rig.

II. MATERIALS AND METHODS

Super 304HCu stainless steel tubes with hardness value of 170 HV and chemical composition as specified in Table 1 is used in this investigation. Samples for air jet erosion test, measuring 20X20X3.5 mm, were extracted from tubes of Super 304HCu in as-received condition. The solid particle air jet erosion tests were performed using an air jet erosion testing apparatus in accordance with the ASTM G76-18 standard, Figure 1.

Table 1: Chemical composition (wt %) of super 304HCu stainless steel.

C	Si	Mn	P	Cr	Ni	N	Cu	Nb
0.09	0.23	0.81	0.021	18.18	9.06	0.095	3.08	0.045

Source: Authors, (2025).

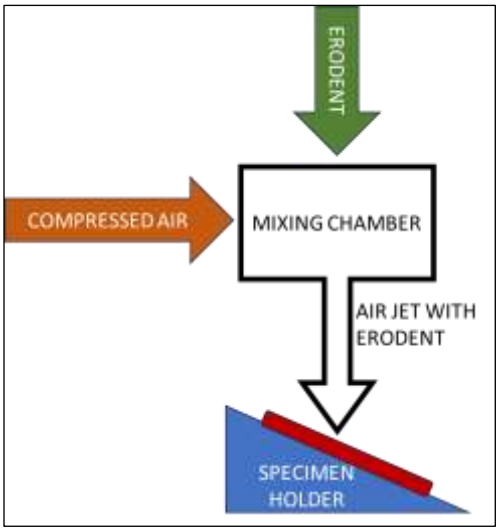

Figure 1: Schematic arrangement of the air jet erosion setup.
Source: Authors, (2025).

Alumina particles of 50 µm (approx.) in size were employed as the solid particle erodent. The rig uses a particle feeder to supply a stream of compressed air jets mixed with erodent particles at high velocity, regulated through a nozzle that is 55 mm long and has an inner diameter of 1.5 mm. A stand-off distance of 10 (+/- 1) mm was maintained between the specimen surface and the nozzle. After accelerating through the nozzle, the particles finally strike the fixed sample on the sample holder. The angle of impact is varied by angling the surface of the sample with respect to the jet direction. The samples were eroded in the rig at different impact angles of study, under a constant impact velocity of 60 m/s and a particle feed rate of 3 g/min, at ambient temperature for 5 minutes (Figure 2).

Figure 2: Photograph of specimens eroded at different angles of impact.
Source: Authors, (2025).

To calculate the weight loss after the erosion test, the samples were cleaned in acetone, dried, and weighed before and after the test. The difference in weight before and after the test was calculated and recorded as the weight loss in the sample per unit weight (g) of the particles used for eroding the sample. The erosion scars of the samples were examined using a macroscope (10X) and the dimensions of the scars were measured using an image analysis software for circularity calculations. Scanning electron microscopy (SEM) was used to study the abrasive scar patterns on the surface of the eroded samples.

III. RESULTS

Figure 3 exhibits the variation in the size and shape of the erosion scar on the sample tested under various angles of impact. The erosion mark is elliptical in shape at lower impact angles and turns to a circular shape as the angle increases to become normal to the impact. The circularity of the erosion scar (C) is calculated using the expression $C=4\pi$ x (A/P^2), where A is area of scar and P is perimeter of the scar [16].

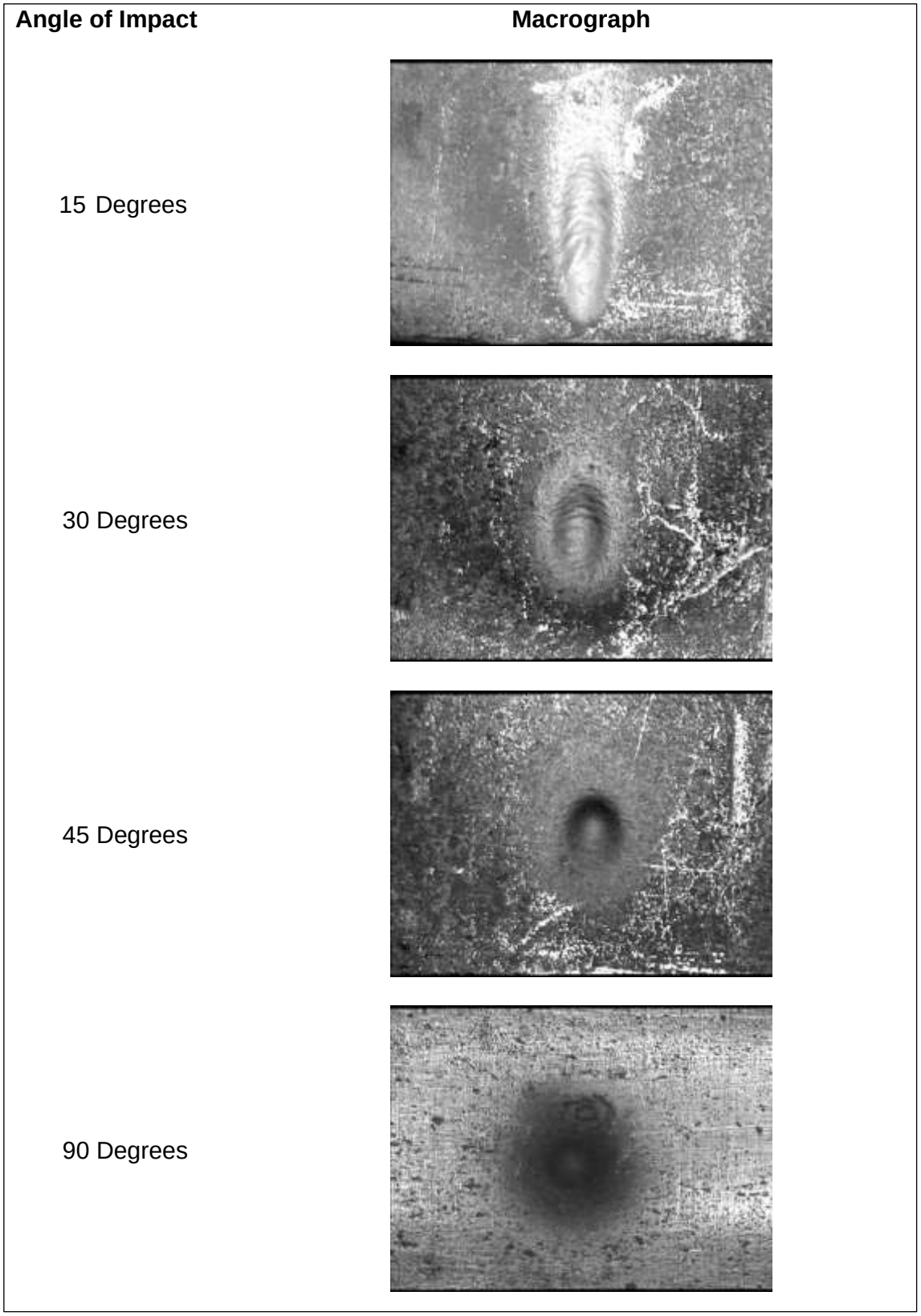

Figure 3: Scanned images of specimen surface eroded at different angles of impact.
Source: Authors, (2025).

Figure 4 depicts the changes in the circularity of the erosion scar at various angles of impact. A circularity value close to unity, depicts a circular scar and a lesser value corresponds to an elliptical scar. The mass loss vs the angle of impact curve (Figure 5a) shows a steep decrease in the mass loss after a 15° angle of impact, while the mass loss remains steady in the impact angles after 30° up to 90°. The mass loss curve of Super 304HCu is typical of a ductile material's erosion behaviour [17]. The mass loss continues to decrease at greater impact angles (>30°), Figure 5b. The test reveals the ductile wear behaviour of Super 304HCu material with a peak erosion rate at a grazing angle (15°), followed by a steep decline with an increase in the angle of impact. The SEM images of the surface of eroded samples at lower and higher angles of impact (Figure 6) reveal the change in erosion mechanisms with change in angle of impact.

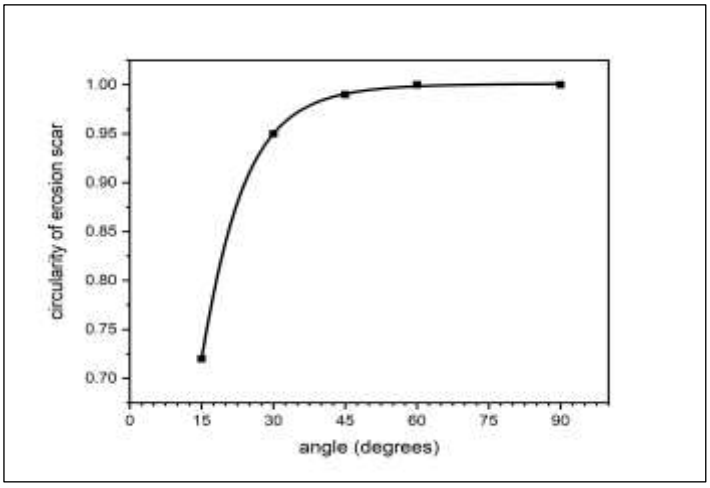

Figure: 4 Relationship graph between the circularity of erosion scar and the angle of impact.
Source: Authors, (2025).

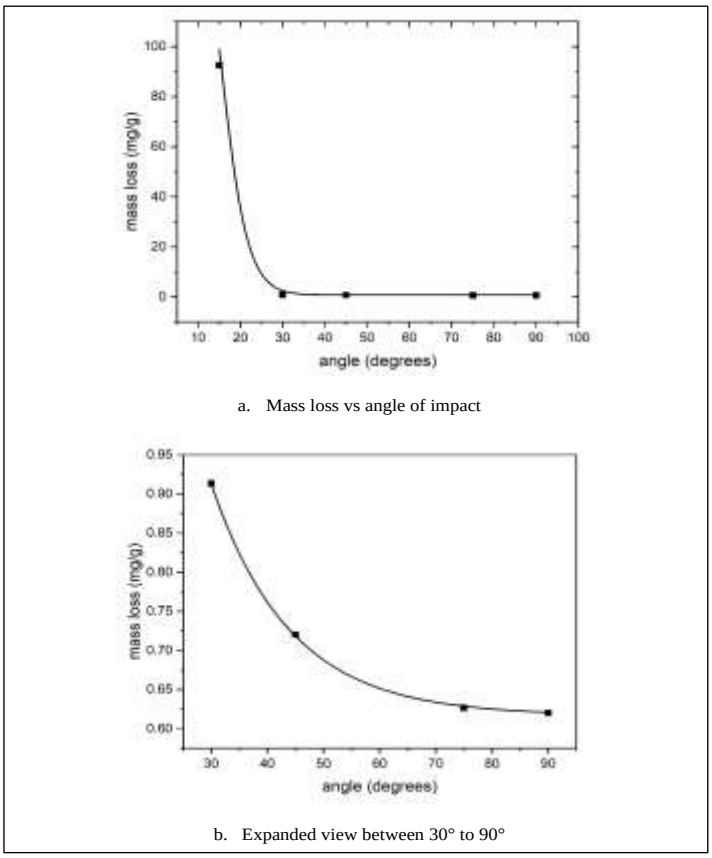

a. Mass loss vs angle of impact

b. Expanded view between 30° to 90°

Figure 5: Relationship graph between the mass loss and angle of impact.
Source: Authors, (2025).

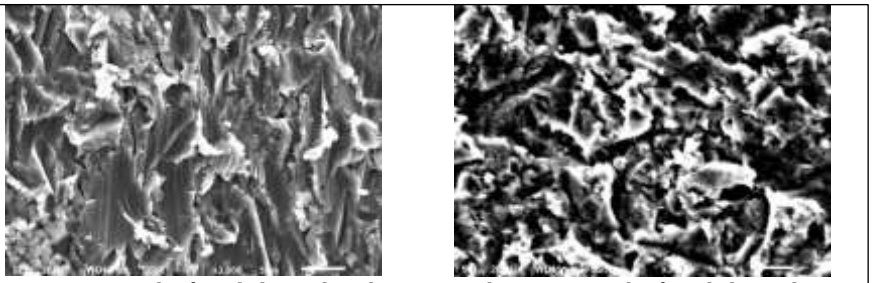

a. Fractograph of eroded sample at low impact angle (15°)

b. Fractograph of eroded sample at high impact angle (90°)

Figure 6: SEM images sample surfaces eroded at different angle of impact.
Source: Authors, (2025).

IV. DISCUSSIONS

The mass loss pattern of Super 304HCu was typical of ductile material and is in compliance with similar grades of stainless steel. The circularity of the scar can provide evidence of the severity of the erosion mechanism active in the region. A less circular, elliptical scar (C<1) can indicate a severe, highly localized erosion of material, aided by the angle of impact. In contrast, a more circular scar (C=1) will be a result of more uniform erosion by the particles impacting the sample normal to the surface, and these particles obstruct the flight path of the particles following them on their rebound, lowering the energy of the impacting particles [18]. The wear surface of the specimen tested at a grazing angle of 15° evidences the extreme ploughing and shear lip formation mechanism by hard abrasive particles active at this angle, along with easy debris removal aided by the lower impact angle, Figure 6a. Meanwhile, the evidence for the lower material loss at higher angles, with mechanisms such as indentation and microcutting, is evidenced in Figure 6b. The normal angle of impact resulted in blunting of wear tracks similar to blasting, inducing compressive stress on the worn surface and thereby decreasing the mass loss at higher angles of impact. The variation in mass loss at different impact angles may also be attributed to the martensite phase transformation of austenite in the eroding region and needs further investigation [6]. The investigation on erosion behaviour of super 304HCu confirmed the large dependence of the angle of impact of erodent on the mass loss of the samples. The mass loss at a gazing angle of 15° was 10 times higher than the mass loss at angles greater than 30°.

V. CONCLUSIONS

The investigation on erosion behaviour of super 304HCu confirmed the large dependence of angle of impact of erodent to the mass loss of the samples. The mass loss was 10 times higher at the gazing angle of 15° than that of the higher angles greater than 30°. The mass loss pattern was typical of ductile material, and is compliant with similar grades of stainless steels.

VI. AUTHOR'S CONTRIBUTION

Conceptualization: M. Balachandar and M. Vinoth Kumar
Methodology: M. Balachandar and M. Vinoth Kumar
Investigation: M. Balachandar and M. Vinoth Kumar
Discussion of results: M. Balachandar and M. Vinoth Kumar
Writing – Original Draft: M. Balachandar and M. Vinoth Kumar
Writing – Review and Editing: M. Balachandar and M. Vinoth Kumar
Resources: M. Balachandar and M. Vinoth Kumar
Supervision: M. Balachandar and M. Vinoth Kumar
Approval of the final text: M. Balachandar and M. Vinoth Kumar

VII. REFERENCES

[1] A. Poonguzhali, N. Babu, G. Shit, and S. Ningshen, "Investigating microstructural and microchemical effect of aging on Cu-rich phase of 304HCu SS exposed to chloride environment by slow strain rate testing technique," *J. Mater. Eng. Perform.*, [Article in Press], 2024.

[2] M. V. Kumar, V. Balasubramanian, and A. G. Rao, "Hot tensile properties and strain hardening behaviour of Super 304HCu stainless steel," *J. Mater. Res. Technol.*, vol. 6, no. 2, pp. 116–122, 2017.

[3] Y. Zhao, C. Tang, J. Yao, and Z. Zeng, "Corrosion behavior of stainless steel in petroleum environments," *Petroleum Sci.*, vol. 17, pp. 1135–1143, 2020.

[4] P. Singh, P. Kumar, and R. L. Virdi, "Erosion and corrosion characteristics of boiler steels," *Mater. Today: Proc.*, vol. 48, pp. 1147–1153, 2021.

[5] J. Yao, F. Zhou, Y. Zhao, H. Yin, and N. Li, "Thermal performance analysis of advanced austenitic steels for high-temperature applications," *Appl. Therm. Eng.*, vol. 88, pp. 353–360, 2025.

[6] P. Singh and S. Mishra, "Erosion behaviour of boiler component materials at room temperature and 400 °C temperature," *Mater. Res. Express*, vol. 7, 2020.

[7] L. Giourntas, T. Hodgkiess, and A. Galloway, "Erosion–corrosion behaviour of engineering alloys at elevated temperatures," *Wear*, vol. 332, pp. 1051–1061, 2015.

[8] M. Bermúdez, F. Carrión, G. M. Nicolás, and R. López, "Erosion–corrosion of steels under slurry impingement conditions," *Wear*, vol. 258, no. 1–4, pp. 693–701, 2005.

[9] Y. Ye, J. Li, X. Lv, and L. Liu, "Erosion–corrosion resistance of metals and alloys in multiphase flow environments," *Metals*, vol. 10, no. 11, p. 1427, 2020.

[10] T. Foley and A. Levy, "Erosion of materials by solid particle impingement at elevated temperatures," *Wear*, vol. 91, no. 1, pp. 45–52, 1983.

[11] C. Morrison, R. Scattergood, and J. Routbort, "Erosion of metallic materials by particle impact," *Wear*, vol. 111, no. 1, pp. 1–10, 1986.

[12] L. Li, L. Li, Z. B. Wang, and Y. Zheng, "Corrosion and oxidation behavior of advanced stainless steels in aggressive environments," *Corros. Sci.*, vol. 158, p. 108084, 2019.

[13] K. Balamurugan, M. Uthayakumar, M. Ramakrishna, and U. Pillai, "Erosion–corrosion characteristics of coated steels in high-temperature service," *Silicon*, vol. 12, pp. 413–420, 2019.

[14] K. Thirugnanasambantham and S. Natarajan, "High temperature erosion–corrosion behaviour of austenitic stainless steels," *J. Mater. Eng. Perform.*, vol. 24, pp. 2605–2614, 2015.

[15] K. Roshan, S. K. Thirumalai, and M. KhanAdam, "Experimental study on solid particle erosion behaviour of stainless steels," *Int. J. Innov. Technol. Explor. Eng.*, vol. 9, pp. 164–170, 2019.

[16] A. Alajmi, B. Hu, and M. Ramulu, “Experimental solid particle erosion of silicon nitride: Optical investigation,” *Ceram. Int.*, vol. 47, pp. 2743–2750, 2021.

[17] M. Divakar, V. Agarwal, and S. N. Singh, “Erosion studies on steels under high-temperature conditions,” *Wear*, vol. 259, pp. 110–118, 2005.

[18] S. Peng, Q. Chen, C. Shan, and D. Wang, “Numerical analysis of particle erosion in the rectifying plate system during shale gas extraction,” *Energy Sci. Eng.*, vol. 7, pp. 1838–1851, 2019.